

Aeroelastic stability consideration of supersonic flight vehicle using nonlinear aerodynamic response surfaces

M. Fathi Jegarkandi^{a,*}, A.S. Nobari^b, M. Sabzehparvar^b, H. Haddadpour^c

^aDepartment of Aerospace Engineering, Amirkabir University of Technology, Tehran, Iran

^bDepartment of Aerospace Engineering and Centre of Excellence in Computational Aerospace Engineering, Amirkabir University of Technology, Tehran, Iran

^cDepartment of Aerospace Engineering, Sharif University of Technology, Tehran, Iran

Received 30 January 2008; accepted 4 April 2009

Available online 30 May 2009

Abstract

Aeroelastic stability of a flexible supersonic flight vehicle is considered using nonlinear dynamics, nonlinear aerodynamics, and a linear structural model. Response surfaces including global multivariate orthogonal modeling functions are invoked to derive applied nonlinear aerodynamic coefficients. A modified Gram–Schmidt method is utilized to orthogonalize the produced polynomial multivariate functions, selected and ranked by predicted squared error metric. Local variation of angle-of-attack and side-slip angle is applied to the analytical model. Identification of nonlinear aerodynamic coefficients of the flight vehicle is conducted employing a CFD code and the required analytical model for simulation purposes is constructed. The method is used to determine the aeroelastic instability and response of a selected flight vehicle.

© 2009 Elsevier Ltd. All rights reserved.

Keywords: Aeroelasticity; Generalized coordinates; Simulation code; Stability; Response surface

1. Introduction

Investigation of the dynamic behavior of a flexible flight vehicle has been the subject on many research works in the field of aeroservoelasticity, which leads to an n -degree of freedom model instead of the 6-degree of freedom models, using the Lagrangian approach.

Meirovitch and Nelson (1966) investigated the stability of spinning elastic flight vehicles by combining flight and elasticity equations based on Lagrange's approach. Considering aeroelastic stability of spinning rockets, Platus (1992) proved that, in some special cases, structural damping can cause instability in spinning vehicles. He used the linear slender body theorem to find the lift force distribution on the considered flight vehicle. Elyada (1989) studied the static aeroelastic instability of non-spinning rockets flying in the plane, just by applying structural effectiveness coefficient in a closed form, without using all necessary equations. Aeroservoelastic instability of an elastic flight vehicle including the related control system was discussed by Haddadpour (2006). He derived equations governing rigid and elastic motions using Lagrange's method. He also applied slender body theory to find lift force distribution on the vehicle.

*Corresponding author. Tel.: +982164543222.

E-mail addresses: phd82129930@aut.ac.ir (M. Fathi Jegarkandi), salehzadeh@cic.ac.ir (A.S. Nobari), sabzeh@cic.ac.ir (M. Sabzehparvar), Haddadpour@sharif.edu (H. Haddadpour).

Nomenclature	
a, b, c, d	Euler parameters
a_j	j th orthogonal function parameter (coefficient of j th orthogonal function in polynomial global model)
A	orthogonal function parameter vector
b_j	j th ordinary polynomial function parameter
B	ordinary polynomial function parameter vector
C	damping coefficient
C_y	side force coefficient
C_z	normal force coefficient
D	aerodynamic reference diameter and damping dissipation function
DERR	contribution of each orthogonal function for the reduction of MSE
\vec{e}	distance vector of each deflected vehicle point from un-deflected one
E	Young's bending modulus
ERR	cumulative sum of DERR
\vec{E}	distance vector of vehicle center of gravity from inertial coordinates origin
EI	flexural rigidity
$f_y(x, t), f_z(x, t)$	distributed side forces along y and z axis
F_x, F_y, F_z	force components along x, y and z axis
F_{Tz}, F_{Ty}, F_{Tx}	thrust force components along x, y and z axis
F_{Az}, F_{Ay}, F_{Ax}	aerodynamic force components along x, y and z axis
GANAM	global analytic nonlinear aerodynamic model
G	Young's torsional modulus
GJ	torsional rigidity
I_y, I_z	moment of inertia about lateral axes
I_x	moment of inertia about longitudinal axis
J	section polar moment of inertia and least squares error cost function
J_i	i th torsional equivalent generalized mass
MSE	mean squared error
r_{wk}	position of k th wing area element relative to its root
dA_{wk}	k th wing area element
x_{wk}	distance of k th wing from body-fixed coordinates origin
x_T	distance of thrust force application point from body-fixed coordinates origin
x_D	distance of resultant aerodynamic force application point from body-fixed coordinates origin
k	wing row identifier
l	number of independent variables
$l_z(x)$	lift force derivative per vehicle length
$l_\beta(x)$	side force derivative per vehicle length
m	flight vehicle mass and number of sample times
$m(x)$	vehicle mass per unit length and distributed moment along longitudinal axis
M_i	i th generalized mass
M_x, M_y, M_z	moment components about x, y and z axis
n	number of retained orthogonal functions
OFFP	over fit penalty
p_j	j th vector orthogonal functions of dimension m
P	$m \times n$ matrix of orthogonal functions
PSE	predicted squared error
p, q, r	angular velocity ($\vec{\omega}$) components about x, y and z axis
\bar{q}	dynamic pressure ($\frac{1}{2}\rho V^2$)
q_i	generalized coordinates and i th vector ordinary polynomial function of dimension m
Q	$m \times n$ matrix of ordinary polynomial functions
Q_i	i th generalized force
r_{kj}	orthogonalization scalar, element of matrix R
\vec{r}	distance vector of each deflected vehicle point from body-fixed coordinates origin
\vec{r}_0	distance vector of each un-deflected vehicle point from body-fixed coordinates origin
\vec{R}	position vector of each deflected vehicle point relative to inertial coordinates origin
R	orthogonalization matrix
t	time
T	kinetic energy
u, v, w	velocity components along x, y and z axis
\vec{V}_I	velocity vector of flight vehicle relative to inertial coordinates
x_i	m -dimensional vector of independent variable i
X	$m \times l$ matrix of independent variable vectors
y_j	i th value of dependent variable
\bar{y}	average value of y_j
x, y, z	body-fixed coordinates
X_I, Y_I, Z_I	inertial coordinates
X_{cg}	change in center of gravity position
α	angle of attack
β	angle of side slip
$\gamma_i, \zeta_i, \eta_i$	generalized coordinates
δ_y, δ_z	lateral elastic deflections
ζ	damping ratio
θ	torsional elastic deflection
$\theta_i(x)$	i th torsional mode shape
μ_i	i th bending mode damping ratio
ν_i	i th torsional mode damping ratio
σ	real part of S
σ_0^2	maximum prediction MSE
$\phi_i(x)$	i th bending mode shape
ψ_i	i th torsional mode frequency
ω	angular velocity
ω_i	i th bending mode frequency

Haddadpour (2006) used modal analysis as well as generalized forces and coordinates to derive the equations of motion in the time domain and then transformed them into the Laplace domain. Utilizing the Routh criterion, he derived an analytic equation in order to analyze elastic stability of slender flight vehicles. Nydick and Friedmann (1998) developed linearized equations of motion using quasi-coordinates to investigate small elastic displacements in pitch and yaw of a supersonic flight vehicle. They utilized nonlinear piston theory in order to determine the aerodynamic lift force. Meirovitch and Tuzcu (2001) developed nonlinear equations of motion using quasi-coordinates and characterized them to implement a computer simulation. They applied strip theory for deriving aerodynamic forces and moments to achieve high computational speed. To investigate the aeroelastic behavior of flight vehicles, Chae and Hodges (2003) developed the equations of motion employing the finite element method to analyze structural flexibility as well as nonlinear slender body and piston theories to derive the aerodynamic forces and moments. Morelli (1995a, b) used multivariate orthogonal modeling functions to drive aerodynamic force and moment coefficients for an F-16 model airplane. In another work by the same author (Morelli, 1995a, b), a similar technique was presented to determine the lift force coefficient using subsonic wind tunnel data for an F-18 HARV airplane and FASER experimental model (Morelli and DeLoach, 2003). A study of the effectiveness of trailing-edge control surfaces has been made for a rolling wing-fuselage model by Tang et al. (2004). An experimental model and wind tunnel tests were used to assess the theoretical results. This theoretical model includes the inherently nonlinear dry friction damping moment that was presented between the spindle support and the experimental aeroelastic wing model. The research provided new insights into the transient dynamic behavior and design of an adaptive wing using trailing- and leading-edge control surfaces. Using flight database for X-29A and X-31A airplanes as well as wind tunnel data for the F-16XL model, applying ordinary least squares method, Klien et al. (1981) identified the aerodynamic force and moment coefficients. A method was proposed by Attar and Dowell (2005) for identifying a set of reduced-order nonlinear equations, which described the structural behavior of aeroelastic configurations. From these equations, zero and nonzero angle of attack flutter and limit-cycle oscillation data were computed for a 45° delta wing aeroelastic model.

In order to investigate the aeroservoelasticity phenomenon using Chebyshev polynomials and their orthogonal properties, Dinu et al. (2006) transformed the unsteady generalized aerodynamic force acting on a fly-by-wire aircraft from reduced frequency domain to the Laplace domain. The mechanism of limit-cycle excitation was investigated for an aeroelastic system with structural nonlinearities (Dessi and Mastroddi, 2008). The analysis was performed on a simplified aeroelastic model retaining only two structural modes (first bending and first torsional modes) and with a simplified description of both unsteady loads due to wing oscillation and external gust excitation. This work deals with the aeroelastic behavior of a small deformed flight vehicle flying at a high angle of attack. A linear structural model is used because of small deformations. The vehicle flies at a high angle of attack, so a nonlinear aerodynamic model must be applied. In this research, integrated equations of motion for an elastic vehicle are developed using Lagrange's approach as well as generalized forces and coordinates. The normal modes of the linear structure are used to determine elastic vibrations. Analytical nonlinear formulations are considered to model the nonlinear aerodynamic force and moment coefficients using orthogonal modeling polynomials developed based on the extracted database from CFD runs. The development of a flight simulation code proceeds using the equations of motion and is executed to investigate aeroelastic stability of a specific supersonic flight vehicle. Finally, the results are verified by comparison with the results of the study of Elyada (1989) and Haddadpour (2006), demonstrating good compatibility between them.

2. Formulation

The general form of Lagrange's equation can be expressed as

$$\frac{d}{dt} \left(\frac{\partial T}{\partial \dot{q}_i} \right) - \frac{\partial T}{\partial q_i} + \frac{\partial U}{\partial q_i} + \frac{\partial D}{\partial \dot{q}_i} = Q_i, \quad (1)$$

where T is kinetic energy, U is potential energy, D is the Rayleigh dissipation damping function and q_i is the i th generalized coordinate. Lagrange's equations in body-fixed coordinates are as follows (Meirovitch and Nelson, 1966):

$$\begin{cases} \frac{d}{dt} \left(\frac{\partial T}{\partial p} \right) - r \frac{\partial T}{\partial q} + q \frac{\partial T}{\partial r} = M_x, \\ \frac{d}{dt} \left(\frac{\partial T}{\partial q} \right) - p \frac{\partial T}{\partial r} + r \frac{\partial T}{\partial p} = M_y, \\ \frac{d}{dt} \left(\frac{\partial T}{\partial r} \right) - q \frac{\partial T}{\partial p} + p \frac{\partial T}{\partial q} = M_z, \end{cases} \quad (2)$$

$$\begin{cases} \frac{d}{dt} \left(\frac{\partial T}{\partial u} \right) - r \frac{\partial T}{\partial v} + q \frac{\partial T}{\partial w} = F_x, \\ \frac{d}{dt} \left(\frac{\partial T}{\partial v} \right) - p \frac{\partial T}{\partial w} + r \frac{\partial T}{\partial u} = F_y, \\ \frac{d}{dt} \left(\frac{\partial T}{\partial w} \right) - q \frac{\partial T}{\partial u} + p \frac{\partial T}{\partial v} = F_z. \end{cases} \quad (3)$$

In Eqs. (2) and (3), (u, v, w) are linear velocities, (p, q, r) are angular velocities, (M_x, M_y, M_z) are moments and (F_x, F_y, F_z) are force components in the body coordinates axis.

Displacements of each element of the vehicle in terms of normal vibration modes are as follows (Bisplinghoff and Ashley, 1962):

$$\theta = \sum_{i=1}^m \theta_i(x) \gamma_i(t), \quad \delta_y = \sum_{i=1}^n \varphi_i(x) \eta_i(t), \quad \delta_z = \sum_{i=1}^p \varphi_i(x) \zeta_i(t), \quad (4)$$

where $\varphi_i(x)$ is the i th normal bending mode shape, $\eta_i(t)$ and $\zeta_i(t)$ are the corresponding generalized coordinates, $\theta_i(x)$ is the i th torsion vibration mode, and $\gamma_i(t)$ is the corresponding generalized coordinate.

If the vehicle is considered as a beam, the bending vibration modes must satisfy the following differential equation (Meirovitch, 1986):

$$\frac{d^2}{dx^2} \left[EI \frac{d^2}{dx^2} \varphi_i(x) \right] = \omega_i^2 m(x) \varphi_i(x), \quad i = 1, 2, 3, \dots, n, \quad (5)$$

where EI is bending stiffness, $m(x)$ is mass distribution per unit length and ω_i is the i th bending mode frequency of the beam. The orthogonality of the vibration modes yields

$$\int_L \varphi_i(x) \varphi_j(x) dm = \begin{cases} 0 & \text{for } i \neq j, \\ M_i & \text{for } i = j, \end{cases} \quad (6)$$

where M_i is the i th generalized mass.

Torsional vibration modes must satisfy the following differential equation (Meirovitch, 1986):

$$\frac{d}{dx} \left(GJ(x) \frac{d\theta_i(x)}{dx} \right) = \rho(x) J(x) \psi_i^2 \theta_i(x), \quad i = 1, 2, 3, \dots, n, \quad (7)$$

where G is shear modulus, $J(x)$ is polar inertial moment of the section, $\rho(x)$ is material density of each section, and ψ_i is the frequency of the i th torsional mode. The orthogonality of the torsional modes leads to:

$$\int \theta_i(x) \theta_j(x) J(x) \rho(x) dx = \begin{cases} 0 & \text{for } i \neq j, \\ J_i & \text{for } i = j, \end{cases} \quad (8)$$

where J_i is the correspondent generalized mass.

Referring to Fig. 1, the displacement of each element of the vehicle regarding to the vibration modes will be as follows:

$$e_x = 0, \quad e_y = \delta_y - z\theta_x = \sum_{i=1}^n (\varphi_i \eta_i - z\theta_i \gamma_i), \quad e_z = \delta_z + y\theta_x = \sum_{i=1}^n (\varphi_i \zeta_i + y\theta_i \gamma_i), \quad (9)$$

where $\delta_x, \delta_y, \delta_z$ are the position vector components of the displaced point after bending, and e_x, e_y and e_z are the position vector components of the displaced point after torsion.

2.1. Kinetic and potential energies and dissipation function

In Fig. 2, the position vector of each point can be expressed as

$$\vec{E} = \vec{R} + \vec{r}, \quad \vec{r} = \vec{r}_0 + \vec{e}, \quad (10)$$

where \vec{E} and \vec{R} are, respectively, the position vectors of center of gravity of the vehicle and each point of the deformed body in inertial coordinates. Also \vec{r}_0 and \vec{r} are the position vectors of each point of the vehicle before and after deformation in the body-fixed coordinates, respectively.

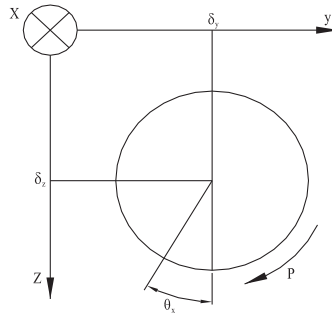


Fig. 1. Section of elastic vehicle in body-fixed coordinates.

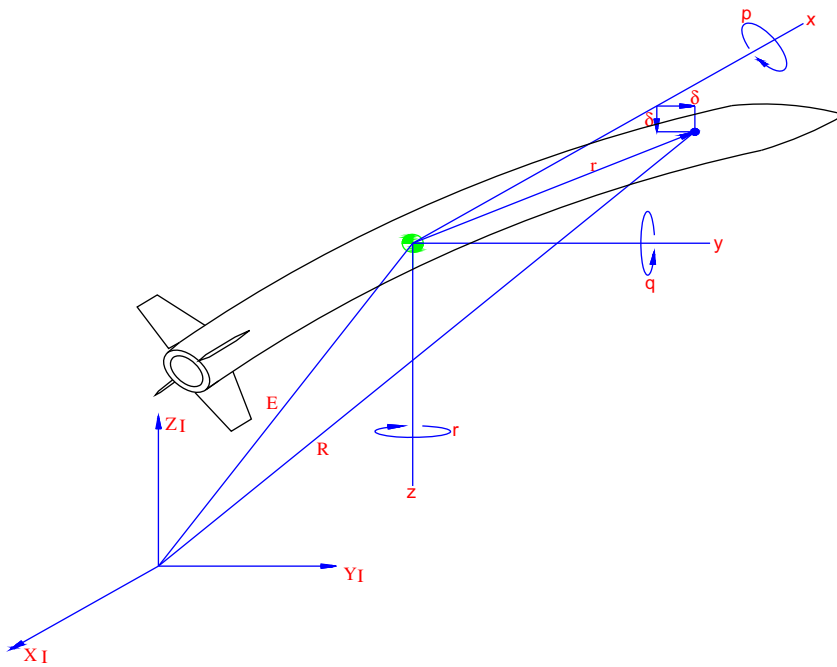


Fig. 2. Inertial and body-fixed coordinates.

The kinetic energy due to rigid and elastic motions is (Meirovitch, 1986)

$$T = \frac{1}{2} \int_m \frac{dE}{dt} \bigg|_I \frac{dE}{dt} \bigg|_I dm = \frac{1}{2} m \vec{V}_I \vec{V}_I + \frac{1}{2} I (r^2 + q^2) + \frac{1}{2} I_x p^2 + \frac{1}{2} \left(p^2 + \frac{q^2 + r^2}{2} \right) \sum_{i=1}^n J_i \dot{\gamma}_i^2 + \frac{1}{2} \sum_{i=1}^n J_i \dot{\gamma}_i^2 + \frac{1}{2} \sum_{i=1}^n M_i [\dot{\eta}_i^2 + \dot{\zeta}_i^2 + p^2 (\zeta_i^2 + \eta_i^2) + (q \zeta_i - r \eta_i)^2 - 2p (\dot{\eta}_i \zeta_i - \dot{\zeta}_i \eta_i)], \quad (11)$$

where I_x and I are the vehicle moments of inertia about longitudinal and lateral axis, respectively.

The potential energy of the beam is expressed as

$$U = \frac{1}{2} \int_L EI \left[\left(\frac{\partial^2 \delta_y}{\partial x^2} \right)^2 + \left(\frac{\partial^2 \delta_z}{\partial x^2} \right)^2 \right] dx + \frac{1}{2} \int_L GJ \left(\frac{\partial \theta}{\partial x} \right)^2 dx. \quad (12)$$

In terms of the modal parameters the potential energy can be written as

$$U = \frac{1}{2} \sum_{i=1}^n M_i \omega_i^2 (\eta_i^2 + \zeta_i^2) + \frac{1}{2} \sum_{i=1}^n J_i \psi_i^2 \gamma_i^2. \quad (13)$$

The Rayleigh dissipation function can be written in terms of the generalized forces and coordinates as follows:

$$D = \frac{1}{2} \sum_{i=1}^n 2\mu_i \omega_i M_i (\dot{\eta}_i^2 + \dot{\zeta}_i^2) + \frac{1}{2} \sum_{i=1}^n 2v_i \psi_i J_i \dot{\gamma}_i^2, \quad (14)$$

where μ_i and v_i are the i th bending and torsion modal damping, respectively. After determination of the kinetic energy, potential energy and Rayleigh dissipation function, the equations of motion can be obtained as discussed in the next section.

2.2. Generalized forces

Generalized forces are on the right-hand side of Lagrange's equations. Assuming that $f_y(x, t)$ is the aerodynamic load distribution on the vehicle in the y direction, the work done due to the virtual displacement $\delta\eta_i$ can be written as follows:

$$\delta W = \int_L f_y(x, t) \sum_{i=1}^n \varphi_i(x) \delta\eta_i(t) dx = \sum_{i=1}^n \delta\eta_i(t) \int_L f_y(x, t) \varphi_i(x) dx. \quad (15)$$

The relation between the generalized force and the virtual work is as

$$Q_{q_i} = \frac{\partial(\delta W)}{\partial(\delta q_i)}. \quad (16)$$

So the generalized forces corresponding to the elastic displacements can be written as

$$Q_{\eta_i} = \int_L f_y(x, t) \varphi_i(x) dx, \quad Q_{\zeta_i} = \int_L f_z(x, t) \varphi_i(x) dx, \quad Q_{\gamma_i} = \int_L m_x(x, t) \theta_i(x) dx, \quad (17, 18, 19)$$

where Q_{η_i} , Q_{ζ_i} , and Q_{γ_i} are the generalized forces, δW is the virtual work and $m_x(x, t)$ is the distributed longitudinal moment.

2.3. Elastic deformations

Using the equations of kinetic and potential energy as well as the virtual work, substituting them into Lagrange's equations and defining η_i , ζ_i , and γ_i as the generalized coordinates, we obtain

$$\ddot{\eta}_i + 2\mu_i \omega_i \dot{\eta}_i - 2p\dot{\zeta}_i + (\omega_i^2 - p^2 - r^2)\eta_i + (qr - \dot{p})\zeta_i = \frac{1}{M_i} \int_L f_y(x, t) \varphi_i(x) dx, \quad (20)$$

$$\ddot{\zeta}_i + 2\mu_i \omega_i \dot{\zeta}_i + 2p\dot{\eta}_i + (\omega_i^2 - p^2 - q^2)\zeta_i + (qr + \dot{p})\eta_i = \frac{1}{M_i} \int_L f_z(x, t) \varphi_i(x) dx, \quad (21)$$

$$\ddot{\gamma}_i + 2v_i \dot{\gamma}_i \psi_i + \left(\psi_i^2 - p^2 - \frac{q^2 + r^2}{2} \right) \gamma_i = \frac{1}{J_i} \int_L m(x, t) \theta_i(x) dx. \quad (22)$$

2.4. Angular velocity equations

Substituting the kinetic energy (Eq. (11)) into Lagrange's equations for the moments (Eq. (2)) and assuming $I_y = I_z = I$, results in

$$\begin{aligned} & \left(I_x + \sum_{i=1}^n J_i \gamma_i^2 + \sum_{i=1}^n M_i (\eta_i^2 + \zeta_i^2) \right) \dot{p} + 2 \left(\sum_{i=1}^n J_i \gamma_i \dot{\gamma}_i + \sum_{i=1}^n M_i (\zeta_i \dot{\zeta}_i + \eta_i \dot{\eta}_i) \right) p \\ & - \sum_{i=1}^n M_i [(\dot{\eta}_i \zeta_i - \dot{\zeta}_i \eta_i) + (q\eta_i - r\zeta_i)(q\dot{\zeta}_i - r\dot{\eta}_i)] = M_x, \end{aligned} \quad (23)$$

$$\begin{aligned} & \left(I - I_m + \sum_{i=1}^n M_i \zeta_i^2 + \frac{1}{2} \sum_{i=1}^n J_i \gamma_i^2 \right) \dot{q} + pr \left(I_x - I + \sum_{i=1}^n M_i \zeta_i^2 + \frac{1}{2} \sum_{i=1}^n J_i \gamma_i^2 \right) \\ & + (pq - \dot{r}) \sum_{i=1}^n M_i \zeta_i \eta_i + 2q \sum_{i=1}^n M_i \zeta_i \dot{\zeta}_i - 2r \sum_{i=1}^n M_i \zeta_i \dot{\eta}_i + q \sum_{i=1}^n J_i \gamma_i \dot{\gamma}_i = M_y, \end{aligned} \quad (24)$$

$$\begin{aligned} & \left(I - I_m + \sum_{i=1}^n M_i \eta_i^2 + \sum_{i=1}^n J_i \gamma_i^2 \right) + pq \left(I - I_x - \sum_{i=1}^n M_i \eta_i^2 - \frac{1}{2} \sum_{i=1}^n J_i \gamma_i^2 \right) \\ & - (pr + \dot{q}) \sum_{i=1}^n M_i \eta_i \zeta_i + 2r \sum_{i=1}^n M_i \eta_i \dot{\eta}_i - 2q \sum_{i=1}^n M_i \dot{\zeta}_i \eta_i + r \sum_{i=1}^n J_i \gamma_i \dot{\gamma}_i = M_z, \end{aligned} \quad (25)$$

where $I_m = mX_{cg}^2$ is due to displacement of instantaneous center of gravity relative to the origin of body-fixed coordinate.

2.5. Equations of angle of attack

Similarly, for the angles of attack, substituting the kinetic energy (Eq. (11)) into Lagrange’s equations for the forces (Eq. (3)), results in

$$m(\dot{u} + qw - rv) = F_{exb}, \quad m(\dot{v} + ru - pw) = F_{eyb}, \quad m(\dot{w} + pv - qu) = F_{ezb}. \quad (26)$$

The forces in the right-hand side of Eq. (26) are derived in the body-fixed coordinate system.

2.6. Moment equations

Moments on the right-hand side of Eqs. (23)–(25) are summations of the external moments due to the aerodynamic lift and thrust forces and can be computed as follows:

$$M_x = - \sum_{k=1}^m \sum_{i=1}^n \int_{A_{w_k}} [l_{\alpha w_k}(r_{w_k}) + l_{\beta w_k}(r_{w_k})] r_{w_k} [p + \dot{\gamma}_i(t) \theta_i(x_{w_k})] dA_{w_k}, \quad (27)$$

$$\begin{aligned} M_y = & - \int x l_{\alpha}(x) \alpha(x, t) dx + \sum_{i=1}^n x_{w_k} l_{\alpha}(x_{w_k}) \alpha(x_{w_k}, t) + F_{Tx} \sum_{i=1}^n \zeta_i(t) \phi_i(x_T) \\ & - F_{Tx} x_T \sum_{i=1}^n \zeta_i(t) \phi_i'(x_T) + F_{Ax} \sum_{i=1}^n \zeta_i(t) \phi_i(x_D), \end{aligned} \quad (28)$$

$$\begin{aligned} M_z = & - \int x l_{\beta}(x) \beta(x, t) dx - \sum_{k=1}^m x_{w_k} l_{\beta}(x_{w_k}) \beta(x_{w_k}, t) - F_{Tx} \sum_{i=1}^n \eta_i(t) \phi_i(x_i) \\ & - F_{Tx} x_T \sum_{i=1}^n \eta_i(t) \phi_i'(x_T) - F_{Ax} \sum_{i=1}^n \eta_i(t) \phi_i(x_D). \end{aligned} \quad (29)$$

2.7. Force equations

Forces on the right-hand side of Eqs. (26) are summations of the aerodynamic lift and thrust forces and are expressed as

$$F_{exb} = F_{Tx} + F_{Ax}, \quad (30)$$

$$F_{eyb} = - \int l_{\beta}(x) \beta(x, t) dx - \sum_{k=1}^m l_{\beta w_k} \beta(x_{w_k}, t) + F_{Tx} \sum_{i=1}^n \eta_i(t) \phi_i'(x_T) + F_{Ax} \sum_{i=1}^n \eta_i(t) \phi_i'(x_D), \quad (31)$$

$$F_{ezb} = - \int l_{\alpha}(x) \alpha(x, t) dx - \sum_{k=1}^m l_{\alpha w_k} \alpha(x_{w_k}, t) + F_{Tx} \sum_{i=1}^n \zeta_i(t) \phi_i'(x_T) + F_{Ax} \sum_{i=1}^n \zeta_i(t) \phi_i'(x_D). \quad (32)$$

2.8. Aeroelastic deflections

Considering Eqs. (17)–(19) and using Eqs. (30)–(32), the generalized forces corresponding to the elastic deflections are derived as follows:

$$\int m(x, t)\theta_i(x)dx = - \sum_{k=1}^m \sum_{i=1}^n \theta_i(x_{w_k}) \int_{A_{w_k}} [l_{\alpha w_k}(r_{w_k}) + l_{\beta w_k}(r_{w_k})]r_{w_k}[p + \dot{\gamma}_i(t)\theta_i(x)]dA_{w_k}, \quad (33)$$

$$\begin{aligned} \int f_y(x, t)\varphi_i(x)dx &= - \int_L l_\beta(x)\beta(x, t)\varphi_i(x)dx - \sum_{k=1}^m \sum_{i=1}^n l_\beta(x_{w_k}, t)\varphi_i(x_{w_k}) \\ &+ F_{Tx} \sum_{i=1}^n \eta_i(t)\varphi'_i(x_T)\varphi_i(x_T) + F_{Ax} \sum_{i=1}^n \eta_i(t)\varphi'_i(x_D)\varphi_i(x_D), \end{aligned} \quad (34)$$

$$\begin{aligned} \int f_z(x, t)\varphi_i(x)dx &= - \int_L l_\alpha(x)\alpha(x, t)\varphi_i(x)dx - \sum_{k=1}^m \sum_{i=1}^n l_\alpha(x_{w_k}, t)\varphi_i(x_{w_k}) \\ &+ F_{Tx} \sum_{i=1}^n \zeta_i(t)\varphi'_i(x_T)\varphi_i(x_T) + F_{Ax} \sum_{i=1}^n \zeta_i(t)\varphi'_i(x_D)\varphi_i(x_D). \end{aligned} \quad (35)$$

Expansion of $\alpha(x, t)$ and $\beta(x, t)$ over the length of the vehicle, and also expansion of $\alpha(x_{w_k}, t)$ and $\beta(x_{w_k}, t)$ at the location of the wings are as follows:

$$\begin{aligned} \alpha(x, t) &= \alpha_0 - \sum_{i=1}^n \zeta_i(t)\varphi'_i(x) + \frac{1}{u} \sum_{i=1}^n \dot{\zeta}_i(t)\varphi_i(x) - \frac{q}{u}x, \\ \beta(x, t) &= \beta_0 - \sum_{i=1}^n \eta_i(t)\varphi'_i(x) + \frac{1}{u} \sum_{i=1}^n \dot{\eta}_i(t)\varphi_i(x) - \frac{r}{u}x, \\ \alpha(x_{w_k}, t) &= \alpha_{0w_k} - \sum_{i=1}^n \zeta_i(t)\varphi'_i(x_{w_k}) + \frac{1}{u} \sum_{i=1}^n \dot{\zeta}_i(t)\varphi_i(x_{w_k}) - \frac{q}{u}x_{w_k}, \\ \beta(x_{w_k}, t) &= \beta_{0w_k} - \sum_{i=1}^n \eta_i(t)\varphi'_i(x_{w_k}) + \frac{1}{u} \sum_{i=1}^n \dot{\eta}_i(t)\varphi_i(x_{w_k}) - \frac{r}{u}x_{w_k}. \end{aligned} \quad (36)$$

Assuming $l_\alpha(x) = l_\beta(x)$, the following parameters are defined as follows:

$$\begin{aligned} \int_L l_\alpha(x)\varphi_i(x)dx &= \int_L xl_\alpha(x)\varphi_i(x)dx = I_1^i, & \int_L xl_\alpha(x)\varphi_i(x)dx &= \int_L xl_\beta(x)\varphi_i(x)dx = I_2^i, \\ \int_L l_\alpha(x)\varphi'_i(x)dx &= \int_L l_\beta(x)\varphi'_i(x)dx = I_3^i, & \int_L xl_\alpha(x)\varphi'_i(x)dx &= \int_L xl_\beta(x)\varphi'_i(x)dx = I_4^i, \\ \int_L l_\alpha(x)\varphi_i^2(x)dx &= \int_L l_\beta(x)\varphi_i^2(x)dx = I_5^i, & \int_L l_\alpha(x)\varphi_i(x)\varphi'_i(x)dx &= \int_L l_\beta(x)\varphi_i(x)\varphi'_i(x)dx = I_6^i. \end{aligned} \quad (37)$$

The above parameters will be used in the compact form of the governing equations of motion.

2.9. Nonlinear aerodynamic modeling

To complete the equations of motion, it is necessary to derive the nonlinear aerodynamic forces and moments. A modeling technique based on the multivariate orthogonal functions is used to develop an accurate analytical model in order to determine aerodynamic coefficients (Morelli, 1995a, 1995b; Morelli and DeLoach, 2003). The required database for developing the model is produced using the CFD method. Each of the aerodynamic coefficients as a dependent variable is determined by using a model including independent variables. Parameters of the model are derived using the least-squares regression method. The model structure is determined by setting the terms of the polynomials and giving priority to them based on the predicted squared error (PSE) metric. The mathematical procedure for deriving multivariate modeling functions will be discussed here. To determine the model structure, an m -dimensional vector of aerodynamic coefficients, as dependent variable values, such as $Y = [y_1, y_2, \dots, y_m]^T$ is assumed

and modeled in terms of a linear combination of n modeling functions $p_j, j = 1, 2, \dots, n$. Each p_j is an m -dimensional vector depended on $X = [x_1, x_2, \dots, x_k]$ and each x_i is an $m \times 1$ vector of the i th independent aerodynamic variable. In the following development, dependence of p_j on x is not explicitly shown in the notation. Then,

$$y = a_1 p_1 + a_2 p_2 + \dots + a_n p_n + \varepsilon, \tag{38}$$

where vector A with components $a_j, j = 1, 2, \dots, n$, includes constant model parameters which should be determined, and ε is the modeling error vector. Defining the vector $P = [p_1, p_2, \dots, p_n]$, where P is an $m \times n$ matrix, and $A = [a_1, a_2, \dots, a_n]^T$, Eq. (38) can be written in matrix form as

$$Y = PA + \varepsilon. \tag{39}$$

The error vector ε should be minimized using the least-squares regression method. The problem is to find a vector A so that it can minimize the following cost function:

$$J = (Y - PA)^T(Y - PA) = \varepsilon^T \varepsilon. \tag{40}$$

The constant-parameter vector, which minimizes the cost function can be estimated using

$$\hat{A} = [P^T P]^{-1} P^T Y. \tag{41}$$

If the ordinary polynomials in the columns of P are nearly linearly dependent, then Eq. (41) will give erroneous estimates of \hat{A} due to ill-conditioning of matrix $P^T P$. The orthogonality of P would have two benefits. Firstly, $P^T P$ would be a diagonal matrix, and the ill-conditioning problem of inverting would be solved. Secondly, the least-squares problem would be decoupled, because each row of Eq. (41) could be solved independently. So, it is required to factorize P into two matrices Q and R , where $Q = [q_1, q_2, \dots, q_n]$ is an $m \times n$ orthogonal matrix and $R = [r_1, r_2, \dots, r_n]$ is an upper triangular $n \times n$ matrix with ones on the diagonal:

$$P = QR, \quad \hat{Y} = P\hat{A} = QR\hat{A}, \tag{42,43}$$

$$\hat{B} = R\hat{A}, \quad \hat{A} = R^{-1}\hat{B}, \quad \hat{Y} = Q\hat{B}. \tag{44,45,46}$$

Now the problem changes to finding the vector B , which minimizes the cost function

$$J = (Y - QB)^T(Y - QB) = \varepsilon^T \varepsilon. \tag{47}$$

The constant-parameter vector, which minimizes the cost function, can be estimated using the following equation:

$$\hat{B} = [Q^T Q]^{-1} Q^T Y. \tag{48}$$

In this situation, each of terms \hat{b}_j , could be determined using the orthogonality condition:

$$q_i^T q_j = 0, \quad i \neq j, \quad i, j = 1, 2, \dots, n. \tag{49}$$

Considering the equation

$$\hat{b}_j = (q_j^T Y) / (q_j^T q_j), \tag{50}$$

indicates that when columns of Q are orthogonal; \hat{b}_j depends only on the measured value of dependent variable or aerodynamic coefficient and its corresponding orthogonal function q_j . Therefore, the model structure could be determined using the contribution of each q_j on the reduction of cost J . In this situation, the estimated cost function could be calculated by

$$\hat{J} = Y^T Y - \sum_{j=1}^n (p_j^T Y)^2 / (p_j^T p_j), \tag{51}$$

where $\text{DERR}_j = (p_j^T Y)^2 / (p_j^T p_j)$ represents the contribution of each term on minimizing the predicted squared error, and ERR denotes the sum $\sum_{j=1}^n \text{DERR}_j$.

The orthogonal functions to be included in the model should be determined based on the contribution of them in minimizing the predicted squared error given in the following equation:

$$\text{PSE} = \text{MSE} + \text{OFP}, \tag{52}$$

where

$$\text{PSE} = (\hat{J}/m) + k\sigma_0^2(n/m), \quad (53)$$

$$\sigma_0^2 = \frac{1}{m} \sum_{i=1}^m (y_i - \bar{y})^2, \quad \bar{y} = \frac{1}{m} \sum_{i=1}^m y_i. \quad (54,55)$$

Eq. (53) indicates that PSE depends on the mean squared error MSE, (\hat{J}/m) , and on a term proportional to the total number of terms in the model, n . The OFP or $k\sigma_0^2(n/m)$ increases by increasing n , and makes the model complex, where MSE decreases by adding each term. Trade-off between these two parameters results in an optimum number of terms, which makes the PSE minimum. It should be mentioned that k must be varied from 9 to 100 to achieve the best fit to the data. To produce the modeling functions matrix P , it is necessary to determine the arrangement of the terms. For example, one common rule for arranging the two variable aerodynamic coefficients with maximum power of k is as follows (Meyer, 1991):

$$C(\alpha, \beta) = \sum_{i=0}^{i+j \leq k} \sum_{j=0} b_{ij} \alpha^i \beta^j. \quad (56)$$

After determining the matrix P and choosing the optimum number of the terms with the aid of PSE metric, it is necessary to find the ranking of the columns by using Error Reduction Index (ERI). ERI is used to rank the orthogonal functions according to their contribution in reducing MSE.

Different techniques are used to produce orthogonal modeling functions. In this research, a two-step procedure based on the Gram–Schmidt orthogonalization method is used (Giraud and Langou, 2002, 2005; Gallivan, 2006). At the first step, modeling functions including independent aerodynamic variables are produced and at the second step, they are orthogonalized using the Gram–Schmidt method.

The orthogonalization process starts with (Morelli, 1995a, b; Morelli and DeLoach, 2003)

$$p_1 = q_1, \quad (57)$$

where q_1 is one of the ordinary polynomial multivariate functions chosen as the first orthogonal function. Usually, q_1 is a $m \times 1$ vector of ones. For making each of columns p_j orthogonal to the preceding orthogonal functions, it must be assumed:

$$p_j = q_j - \sum_{k=1}^{j-1} r_{kj} p_k, \quad j = 2, 3, \dots, n, \quad (58)$$

where r_{kj} are scalars determined by

$$r_{kj} = \frac{p_k^T q_j}{p_k^T p_k}, \quad k = 1, 2, \dots, (j-1), \quad j = 2, 3, \dots, n. \quad (59)$$

3. Summary of equations

In order to track the path of the vehicle, the translational equations of motion of the vehicle must be transferred from body-fixed coordinate system to inertial coordinate system by using a transfer function for transferring \vec{F}_B to \vec{F}_I as follows:

$$\vec{F}_I = C_B^I \vec{F}_B. \quad (60)$$

Using Euler parameters one can write C_B^I as follows:

$$C_B^I = \begin{bmatrix} a^2 + b^2 + c^2 - d^2 & 2(bc - ad) & 2(ac + bd) \\ 2(ad + bc) & a^2 - b^2 + c^2 - d^2 & 2(cd - ab) \\ 2(db - ac) & 2(ab + cd) & a^2 - b^2 - c^2 + d^2 \end{bmatrix}, \quad (61)$$

where a, b, c and d , are the Euler parameters (quaternions), are defined as:

$$a = \cos\left(\frac{\delta}{2}\right), \quad \vec{p} = \begin{bmatrix} b \\ c \\ d \end{bmatrix} = \sin\left(\frac{\delta}{2}\right) \vec{u}_\delta, \quad (62)$$

where \bar{u}_δ is the unit vector on the axis of rotation and δ is the magnitude of rotation. Also we have the following relation between the Euler parameters which adds an equation for determining the redundant variable:

$$a^2 + \langle \bar{p}, \bar{p} \rangle = a^2 + b^2 + c^2 + d^2 = \cos^2\left(\frac{\delta}{2}\right) + \sin^2\left(\frac{\delta}{2}\right) = 1. \tag{63}$$

By using the above definitions for driving forces in inertial coordinates we shall have

$$\begin{bmatrix} F_{xI} \\ F_{yI} \\ F_{zI} \end{bmatrix} = C_B^I \begin{bmatrix} F_{exb} \\ F_{eyb} \\ F_{ezb} \end{bmatrix} + \begin{bmatrix} F_{Gx} \\ F_{Gy} \\ F_{Gz} \end{bmatrix}. \tag{64}$$

Finally, the state differential equations will be as follows:

$$\dot{X}(t) = V_X, \quad \dot{Y}(t) = V_Y, \quad \dot{Z}(t) = V_Z, \tag{65}$$

$$\dot{V}_x(t) = F_{xI}/m, \quad \dot{V}_y(t) = F_{yI}/m, \quad \dot{V}_z(t) = F_{zI}/m, \tag{66}$$

$$\dot{p}(t) = \left[M_{Ax} + M_{Tx} + \sum_{k=1}^m \sum_{i=1}^n l_{P_{wk}} \dot{\gamma}_i(t) \theta_i(x_{wk}) \right] / I_x, \tag{67}$$

$$\begin{aligned} \dot{q}(t) = & \left[M_{Ay} + (I - I_x - I_m)pr + M_{Ty} - qF_{J2} + X_{cg}F_{ezb} - I_4^i \sum_{i=1}^n \zeta_i(t) + \frac{1}{u} I_2^i \sum_{i=1}^n \dot{\zeta}_i(t) \right. \\ & - \sum_{k=1}^m \sum_{i=1}^n x_{wk} l_{zwk}(x_{wk}) \phi'_i(x_{wk}) \zeta_i(t) + \frac{1}{u} \sum_{k=1}^m \sum_{i=1}^n x_{wk} l_{zwk}(x_{wk}) \phi_i(x_{wk}) \dot{\zeta}_i(t) \\ & \left. + \sum_{i=1}^n \zeta_i(t) \phi_i(x_T) F_{Tx} - \sum_{i=1}^n \zeta_i(t) \phi'_i(x_T) x_T F_{Tx} + \sum_{i=1}^n \zeta_i(t) \phi_i(x_D) F_{Ax} \right] / (I - I_m), \end{aligned} \tag{68}$$

$$\begin{aligned} \dot{r}(t) = & \left[M_{Az} + (I_x - I + I_m)pq + M_{Tz} - rF_{J2} + X_{cg}F_{ezb} + I_4^i \sum_{i=1}^n \eta_i(t) - \frac{1}{u} I_2^i \sum_{i=1}^n \dot{\eta}_i(t) \right. \\ & + \sum_{k=1}^m \sum_{i=1}^n x_{wk} l_{\beta wk}(x_{wk}) \phi'_i(x_{wk}) \eta_i(t) - \frac{1}{u} \sum_{k=1}^m \sum_{i=1}^n x_{wk} l_{\beta wk}(x_{wk}) \phi_i(x_{wk}) \dot{\eta}_i(t) \\ & \left. - \sum_{i=1}^n \eta_i(t) \phi_i(x_T) F_{Tx} + \sum_{i=1}^n \eta_i(t) \phi'_i(x_T) x_T F_{T(x)} - \sum_{i=1}^n \eta_i(t) \phi_i(x_D) F_{Ax} \right] / (I - I_m), \end{aligned} \tag{69}$$

$$\begin{aligned} \ddot{\zeta}_i(t) = & \frac{1}{M_i} \left[-\alpha_0 I_1^i + \sum_{i=1}^n \zeta_i(t) I_6^i - \frac{1}{u} \sum_{i=1}^n \dot{\zeta}_i(t) I_5^i + \frac{q}{u} I_2^i - \sum_{k=1}^m \sum_{i=1}^n l_{zwk}(x_{wk}) \alpha_{0wk} \phi_i(x_{wk}) \right. \\ & + \sum_{k=1}^m \sum_{i=1}^n l_{zwk}(x_{wk}) \phi_i(x) \phi'_i(x) \zeta_i(t) - \frac{1}{u} \sum_{k=1}^m \sum_{i=1}^n l_{zwk}(x_{wk}) \phi_i^2(x_{wk}) \dot{\zeta}_i(t) \\ & + \frac{q}{u} \sum_{k=1}^m \sum_{i=1}^n x_{wk} l_{zwk}(x_{wk}) \phi_i(x_{wk}) + \sum_{i=1}^n \zeta_i(t) \phi_i(x_T) \phi'_i(x_T) F_{Tx} \\ & \left. + \sum_{i=1}^n \zeta_i(t) \phi_i(x_D) \phi'_i(x_D) F_{Ax} \right] - 2\mu_i \omega_i \dot{\zeta}_i(t) - 2p\dot{\eta}(t) - (\omega_i^2 - p^2) \zeta_i(t), \end{aligned} \tag{70}$$

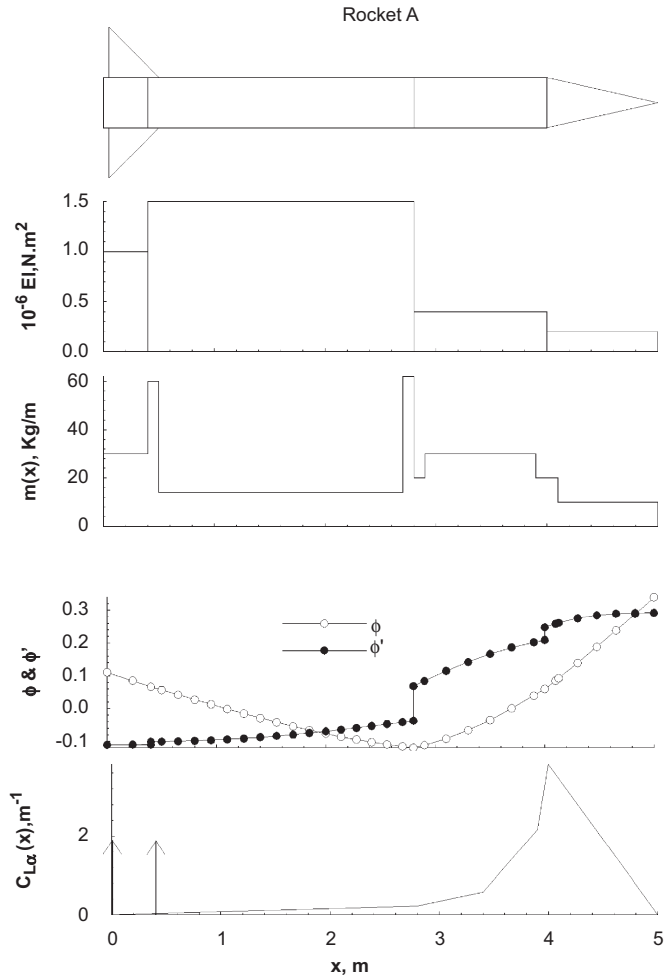


Fig. 3. Distributed properties of the vehicle A.

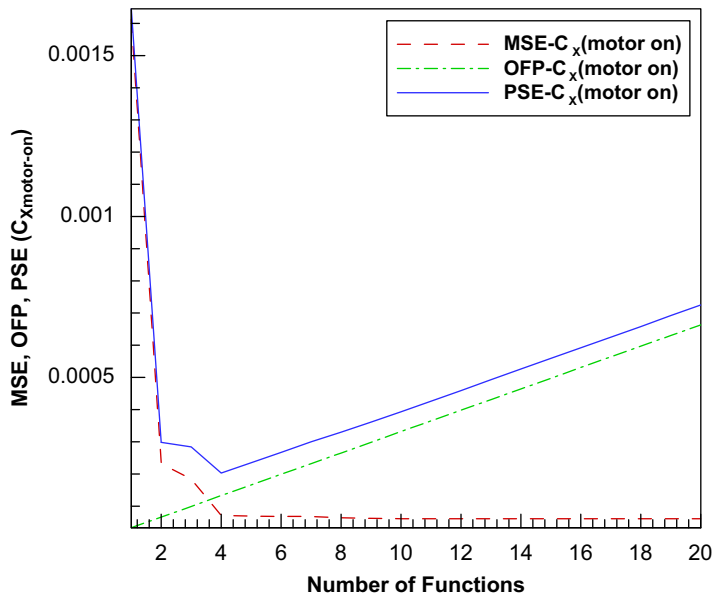


Fig. 4. MSE, OFP, PSE versus number of functions for $(C_x)_{motor-on}$.

$$\ddot{\eta}_i(t) = \frac{1}{M_i} \left[-\beta_0 I_1^i + \sum_{i=1}^n \eta_i(t) I_6^i - \frac{1}{u} \sum_{i=1}^n \dot{\eta}_i(t) I_5^i + \frac{r}{u} I_2^i - \sum_{k=1}^m \sum_{i=1}^n l_{\beta w_k}(x_{w_k}) \beta_{0w_k} \varphi_i(x_{w_k}) \right. \\ + \sum_{k=1}^m \sum_{i=1}^n l_{\beta w_k}(x_{w_k}) \varphi_i(x) \varphi_i'(x) \eta_i(t) - \frac{1}{u} \sum_{k=1}^m \sum_{i=1}^n l_{\beta w_k}(x_{w_k}) \varphi_i^2(x_{w_k}) \dot{\eta}_i(t) \\ + \frac{r}{u} \sum_{k=1}^m \sum_{i=1}^n x_{w_k} l_{\beta w_k}(x_{w_k}) \varphi_i(x_{w_k}) + \sum_{i=1}^n \eta_i(t) \varphi_i(x_T) \varphi_i'(x_T) F_{Tx} + \sum_{i=1}^n \eta_i(t) \varphi_i(x_T) \varphi_i'(x_T) F_{Tx} \\ \left. + \sum_{i=1}^n \eta_i(t) \varphi_i(x_D) \varphi_i'(x_D) F_{Ax} \right] - 2\mu_i \omega_i \dot{\eta}_i(t) - 2p \zeta_i(t) - (\omega_i^2 - p^2) \eta_i(t), \tag{71}$$

$$\ddot{\gamma}_i(t) = \frac{1}{J_i} \left[M_{Ax} + \sum_{k=1}^m \sum_{i=1}^n l_{p w_k} \theta_i^2(x_{w_k}) \dot{\gamma}_i(t) \right] - 2\nu_i \psi_i \dot{\gamma}_i(t) - (\psi_i^2 - p^2) \gamma_i(t), \tag{72}$$

Table 1
Number of the terms included in the model for $(C_x)_{\text{motor-on}}$.

N	Term	MSE	OFP	PSE	J-hat	ERR
1	1	0.001612	0.000033	0.001645	2.349650	85.525373
2	M	0.000232	0.000066	0.000298	0.337939	87.537085
3	M ³	0.000184	0.000099	0.000284	0.268659	87.606365
4	M ²	0.000071	0.000133	0.000203	0.103312	87.771712
5	α ² M	0.000069	0.000166	0.000235	0.101219	87.773805
6	αβM	0.000068	0.000199	0.000267	0.099861	87.775162
7	β ² M	0.000068	0.000232	0.000300	0.098969	87.776055
8	α ²	0.000064	0.000265	0.000330	0.093660	87.781364
9	αβ	0.000062	0.000298	0.000361	0.090979	87.784045
10	β ²	0.000061	0.000332	0.000393	0.089628	87.785396

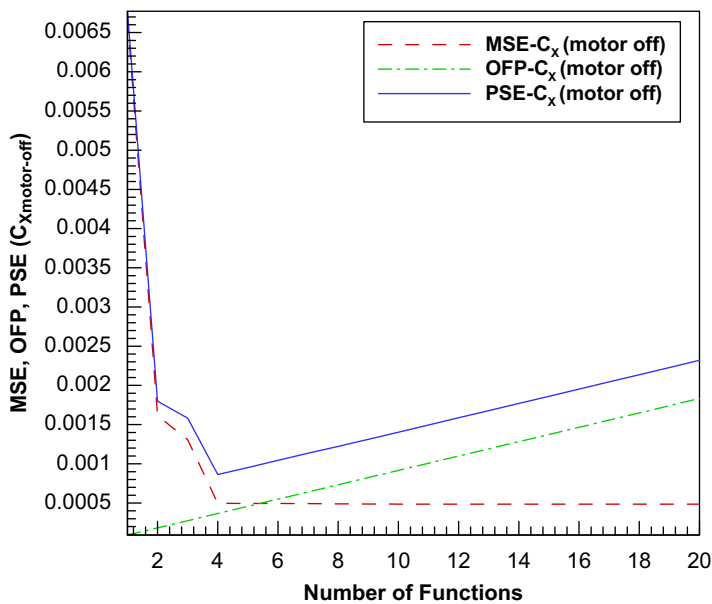


Fig. 5. MSE, OFP, PSE versus number of functions for $(C_x)_{\text{motor-off}}$.

Table 2
Number of the terms included in the model for $(C_X)_{\text{motor-off}}$.

n	Term	MSE	OFP	PSE	J-hat	ERR
1	1	0.006680	0.000092	0.006771	9.739185	196.288932
2	M	0.001616	0.000183	0.001799	2.356333	203.671784
3	M^2	0.001308	0.000275	0.001583	1.907431	204.120686
4	M^2	0.000496	0.000367	0.000863	0.723770	205.304347
5	$\alpha^2 M$	0.000495	0.000458	0.000953	0.721686	205.306431
6	$\alpha\beta M$	0.000494	0.000550	0.001044	0.720330	205.307787
7	$\beta^2 M$	0.000493	0.000641	0.001135	0.719446	205.308671
8	α^2	0.000490	0.000733	0.001223	0.714145	205.313972
9	$\alpha\beta$	0.000488	0.000825	0.001313	0.711463	205.316654
10	β^2	0.000497	0.000916	0.001403	0.710119	205.317999

Table 3
Number of the terms included in the model for C_Y .

n	Term	MSE	OFP	PSE	J-hat	ERR
1	β	0.053009	0.001940	0.054950	77.287366	1985.133963
2	α	0.048599	0.003881	0.052480	70.857963	1991.563366
3	βM	0.024507	0.005821	0.030329	35.732001	2026.689329
4	αM	0.023574	0.007762	0.031336	34.371305	2028.050024
5	$\alpha\beta^2$	0.023458	0.009702	0.033160	34.202383	2028.218946
6	αM^2	0.022786	0.011642	0.034429	33.222155	2029.199174
7	βM^2	0.022282	0.013583	0.035864	32.486638	2029.934691
8	$<\beta^3$	0.020616	0.015523	0.036140	30.058802	2032.362527
9	$<\alpha^3$	0.020223	0.017464	0.037686	29.484693	2032.936636
10	$\alpha^2\beta$	0.019829	0.019404	0.039233	28.910805	2033.510524

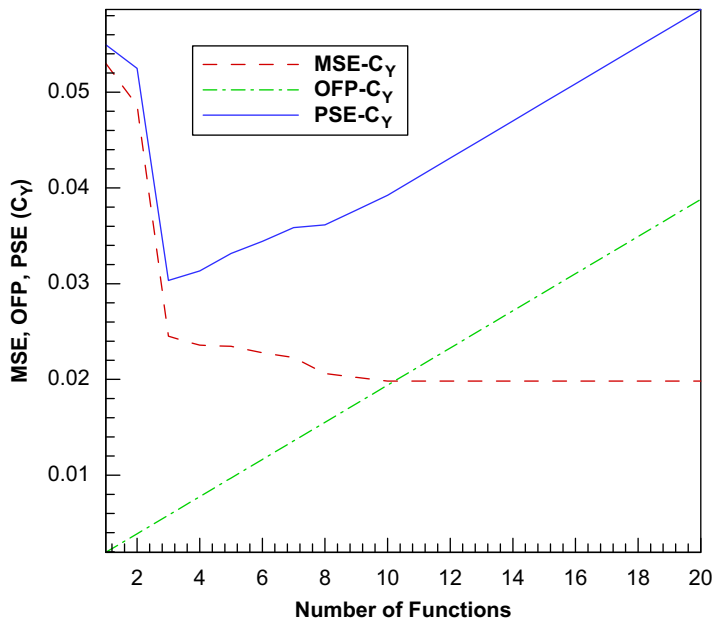


Fig. 6. MSE, OFP, PSE versus number of functions for C_Y .

$$\dot{a}(t) = -\frac{1}{2}[b(t)p(t) + c(t)q(t) + d(t)r(t)], \quad \dot{b}(t) = \frac{1}{2}[a(t)p(t) + c(t)r(t) - d(t)q(t)], \tag{73,74}$$

$$\dot{c}(t) = \frac{1}{2}[a(t)q(t) - b(t)r(t) + d(t)p(t)], \quad \dot{d}(t) = \frac{1}{2}[a(t)r(t) + b(t)q(t) - c(t)p(t)]. \tag{75,76}$$

The above nonlinear equations define flight vehicle motions. By solving the equations using the fourth-order Runge–Kutta method, positions as well as angular and linear velocities and accelerations of the flight vehicle will be determined.

4. Results

In order to verify the approach used, we made aeroservoelastic calculations for some test cases. The first case was generated by applying GANAM to the data produced from CFD code for ‘vehicle A’ (Elyada, 1989; Haddadpour, 2006), as presented in Fig. 3.

Table 4
Number of the terms included in the model for C_z .

n	Term	MSE	OFP	PSE	J-hat	ERR
1	α	0.053009	0.001940	0.054950	77.287345	1985.134355
2	αM	0.028920	0.003881	0.032801	42.165587	2020.256113
3	β	0.024508	0.005821	0.030329	35.731992	2026.689708
4	α^3	0.022939	0.007762	0.030701	33.445104	2028.976596
5	αM^2	0.021768	0.009702	0.031470	31.737914	2030.683786
6	βM	0.020835	0.011642	0.032447	30.376861	2032.044840
7	$\alpha\beta^2$	0.020175	0.013583	0.033758	29.415063	2033.006638
8	$\alpha^2\beta$	0.019837	0.015523	0.035360	28.922722	2033.498979
9	βM^2	0.019831	0.017464	0.037295	28.913622	2033.508078
10	β^3	0.019829	0.019404	0.039233	28.910851	2033.510850

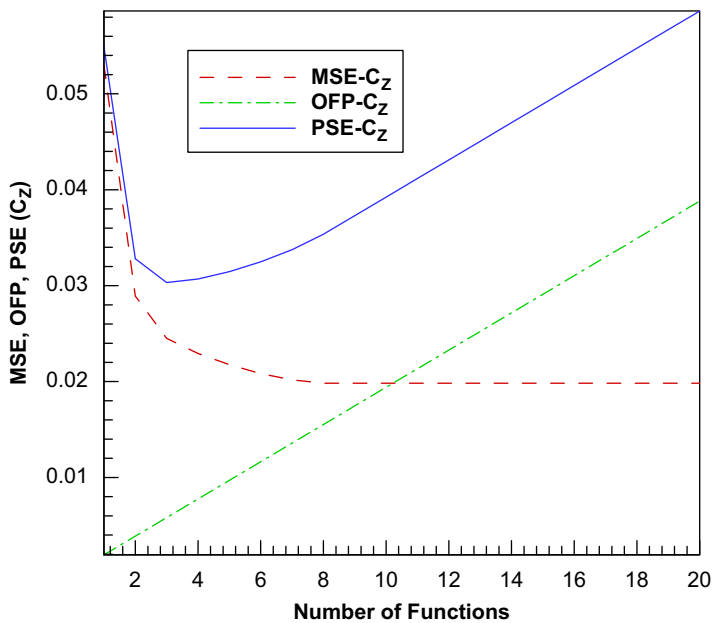


Fig. 7. MSE, OFP, PSE versus number of functions for C_z .

The aerodynamic force and moment coefficients are derived as follows. The $(C_X)_{\text{motor-on}}$ coefficient is used to compute the axial aerodynamic force during the powered flight of the vehicle. The numerical values of the model, fitting errors, MSE, OFP, and PSE for the coefficient $(C_X)_{\text{motor-on}}$, are given in Table 1. ERR represents the contribution of the total number of terms in MSE reduction. Variations of MSE, OFP, and PSE versus the number of used orthogonal modeling functions for the coefficient $(C_X)_{\text{motor-on}}$ are plotted in Fig. 4. This model is considered with a maximum power of three. So, the total number of the functions used will be 20. However, just the first 10 terms are ranked in Table 1. As indicated in Table 1 and Fig. 4, just four terms are enough to minimize PSE metric for the model. The resultant GANAM for this coefficient would be as follows:

$$(C_X)_{\text{motor-on}} = 0.2650 + 0.0402M + 0.0032M^3 - 0.0285M^2. \tag{77}$$

The Coefficient $(C_X)_{\text{motor-off}}$ is used to compute the axial aerodynamic force during powered flight of the vehicle. Numerical values of MSE, OFP, and PSE for the coefficient $(C_X)_{\text{motor-off}}$ are shown in Table 2. Variations of MSE, OFP, and PSE versus the number of used orthogonal modeling functions for the coefficient $(C_X)_{\text{motor-off}}$ are plotted in Fig. 5. Just the first 10 terms of the model are ranked in Table 2. The resultant GANAM for this coefficient would be as follows:

$$(C_X)_{\text{motor-off}} = 0.3757 + 0.1323M + 0.0087M^3 - 0.0762M^2. \tag{78}$$

Table 5
Number of the terms included in the model for C_l .

n	Term	MSE	OFP	PSE	J-hat	ERR
1	α^2	0.003939	0.000157	0.004096	5.743398	0.936591
2	$\alpha\beta$	0.002681	0.000314	0.002995	3.908571	2.771418
3	β^2	0.001868	0.000471	0.002340	2.723926	3.956063
4	α^2M	0.001840	0.000628	0.002469	2.682938	3.997051
5	$\alpha\beta M$	0.001785	0.000786	0.002571	2.602501	4.077488
6	$\beta^2 M$	0.001749	0.000943	0.002692	2.550651	4.129338
7	αM	0.001749	0.001100	0.002849	2.550651	4.129338
8	α	0.001749	0.001257	0.003006	2.550651	4.129338
9	M^3	0.001749	0.001414	0.003163	2.550651	4.129338
10	1	0.001749	0.001571	0.003321	2.550651	4.129338

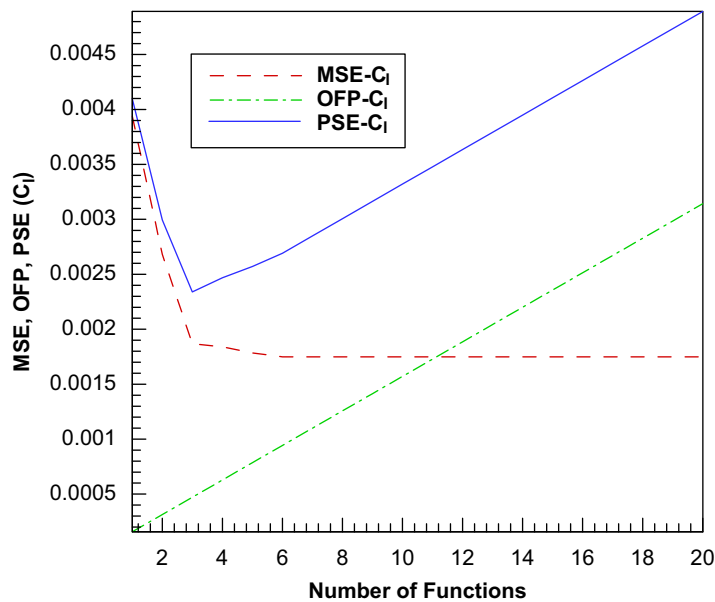


Fig. 8. MSE, OFP, PSE versus number of functions for C_l .

Table 3 shows the numerical values of MSE, OFP, and PSE for the coefficient C_Y . Variations of MSE, OFP, and PSE versus the number of used orthogonal modeling functions for the coefficient C_Y are plotted in Fig. 6. Just the first 10 terms of the model are ranked in Table 3. It can be seen from the model that, for this special symmetric vehicle, the coefficient C_Y vanishes at zero angles of attack and side slip. The resultant GANAM for this coefficient would be as follows:

$$C_Y = -17.3014\beta + 1.1288\alpha + 1.1980\beta M. \tag{79}$$

The numerical values of MSE, OFP, and PSE for the coefficient C_Z are shown in Table 4. Variations of MSE, OFP, and PSE versus the number of used orthogonal modeling functions for the coefficient C_Z have been plotted in Fig. 7. By considering symmetry about Y and Z axis, and replacing α by β and *vice versa* in the model of C_Y , this method gives the same model for C_Z but with opposite sign for the fitting error parameters and polynomial coefficients.

This model is considered with maximum power of three. So, the total number of the functions will be twenty. However, just the first 10 terms are ranked in Table 4.

Table 6
Number of the terms included in the model for C_m .

n	Term	MSE	OFP	PSE	J-hat	ERR
1	α	12.551626	0.195724	12.747350	18300.270864	23306.037312
2	αM	3.265579	0.391448	3.657027	4761.214871	36845.093305
3	β	2.653936	0.587172	3.241109	3869.440116	37736.868060
4	$\alpha\beta^2$	2.331716	0.782896	3.114613	3399.642617	38206.665559
5	$\alpha^2\beta$	2.292623	0.978620	3.271243	3342.644298	38263.663878
6	αM^2	2.136189	1.174344	3.310533	3114.563265	38491.744911
7	βM	2.092422	1.370068	3.462490	3050.751689	38555.556487
8	α^3	2.085054	1.565792	3.650846	3040.008367	38566.299809
9	βM^2	2.082262	1.761516	3.844423	3036.877404	38569.430772
10	β^3	2.610216	1.957240	4.039502	3035.937732	38570.370444

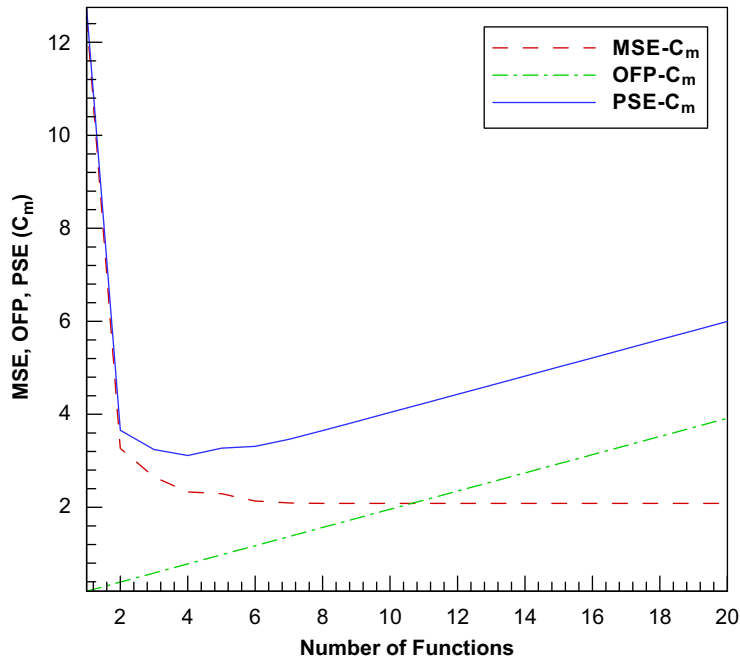


Fig. 9. MSE, OFP, PSE versus number of functions for C_m .

As can be seen from Table 4 and Fig. 7, three terms are enough to minimize PSE metric for the model. The resultant GANAM for this coefficient would be as follows:

$$C_Z = 17.3014\alpha - 1.1980\alpha M - 1.1288\beta. \tag{80}$$

The numerical values of MSE, OFP, and PSE for the coefficient C_Y are shown in Table 5. Variations of MSE, OFP, and PSE have been plotted in Fig. 8. Just the first 10 terms of the model are ranked in Table 5. As can be seen in Table 5 and Fig. 8, three terms are enough to minimize PSE metric for the model. However, the simplest model is achieved by trying with two terms and ignoring the second term because of its small effect. The resultant GANAM for this coefficient would be as follows:

$$C_I = 5.6289\alpha^2 - 5.6289\beta^2. \tag{81}$$

For the coefficient C_m , the numerical values of MSE, OFP, and PSE are shown in Table 6. Variations of MSE, OFP, and PSE versus number of orthogonal modeling functions for C_m have been plotted in Fig. 9. Just the first 10 terms are

Table 7
Number of the terms included in the model for C_n .

n	Term	MSE	OFP	PSE	J-hat	ERR
1	β	12.551627	0.195724	12.747351	18300.272431	23306.033282
2	βM	3.265582	0.391448	3.657030	4761.218057	36845.087656
3	α	2.653938	0.587172	3.241111	3869.442325	37736.863838
4	αM	2.610218	0.782896	3.393114	3805.697389	37800.608323
5	α^3	2.439302	0.978620	3.417922	3556.501887	38049.803825
6	$\alpha^2\beta$	2.276409	1.174344	3.450753	3319.003909	38287.301803
7	αM^2	2.179049	1.370068	3.549117	3177.053791	38429.251922
8	βM^2	2.117844	1.565792	3.683637	3087.817227	38518.488485
9	β^2	2.089814	1.761516	3.851330	3046.948501	38559.357211
10	β^3	2.082263	1.957240	4.039503	3035.939383	38570.366330

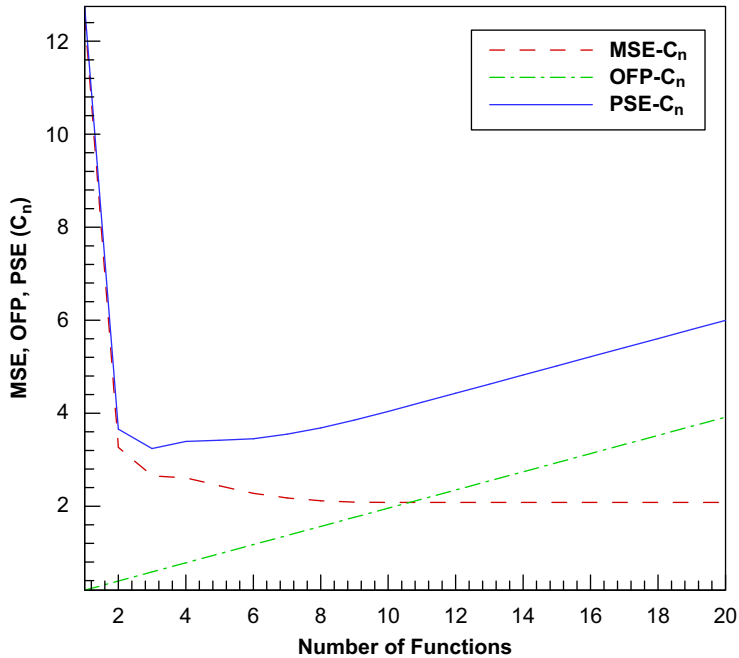


Fig. 10. MSE, OFP, PSE versus number of functions for C_n .

ranked in Table 6. The resultant analytical global nonlinear model for this coefficient would be as follows:

$$C_m = -105.8426\alpha + 23.5200\alpha M + 13.2895\beta. \tag{82}$$

The numerical values of MSE, OFP, and PSE for the coefficient C_n have been shown in Table 7 showing only the first ten terms. Variations of MSE, OFP, and PSE versus number of orthogonal modeling functions for the coefficient C_n have been plotted in Fig. 10. In this case, again, by considering the vehicle symmetry about Y and Z axis, and replacing α by β and vice versa, the method gives the same model for C_n but with opposite sign in parameters and polynomial coefficients of C_m . The resultant GANAM for this coefficient would be as follows:

$$C_n = 105.8426\beta - 23.5200\beta M - 13.2895\alpha. \tag{83}$$

To avoid repetition of similar sentences, maximum power of the modeling functions, total number of the terms, and minimum number of the functions required for minimizing PSE metric for each coefficient are summarized in Table 8.

After completing the modeling procedure and deriving coupled equations of flight dynamics, aeroelasticity and GANAM, and aeroelastic flight simulation is executed for 'vehicle A'. Results of flight simulation for the vehicle are shown in Figs. 11–15.

Table 8

Maximum power, total number of terms in the model and minimum number of the functions required for minimizing PSE.

Coefficient	Maximum power	Total number	Minimum number
$(C_X)_{\text{motor-on}}$	3	20	4
$(C_X)_{\text{motor-off}}$	3	20	4
C_Y	3	20	3
C_Z	3	20	3
C_l	3	20	2
C_m	3	20	3
C_n	3	20	3

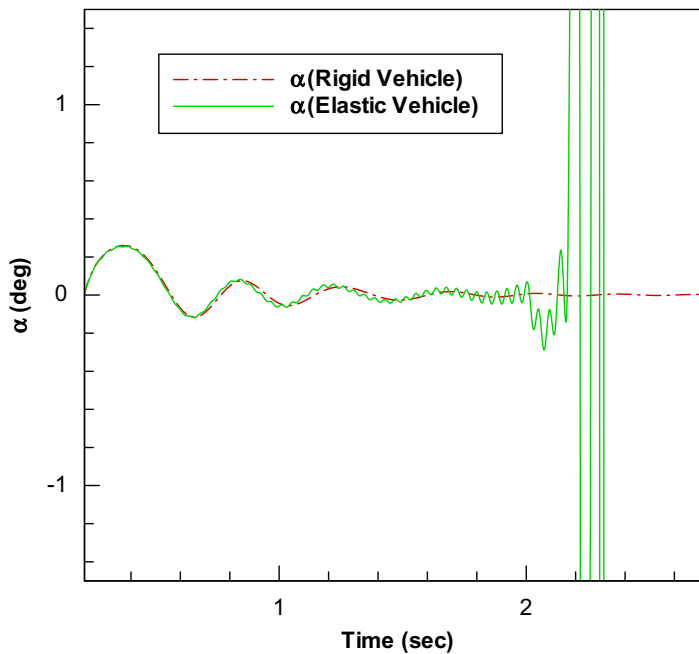


Fig. 11. Angle of attack for rigid and elastic vehicles.

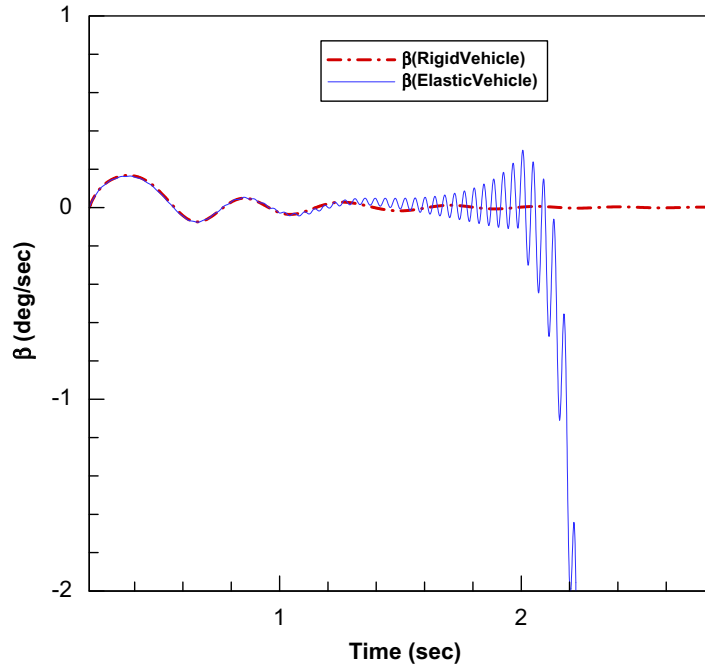


Fig. 12. Angle of side slip for rigid and elastic vehicles.

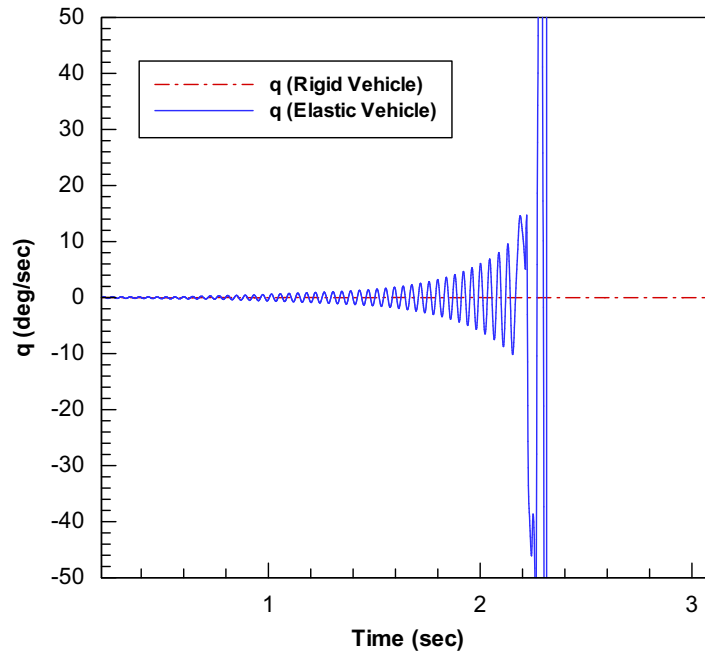


Fig. 13. Pitch angular velocity for rigid and elastic vehicles.

Variations in the angle of attack for rigid and elastic vehicles are shown in Fig. 11. As the figure obviously indicates, the oscillation amplitude of the angle of attack increases in the elastic case and the vehicle diverges from its flight path. Structural flexibility decreases the static margin from about $2.12D$ to zero and consequently decreases the static stability

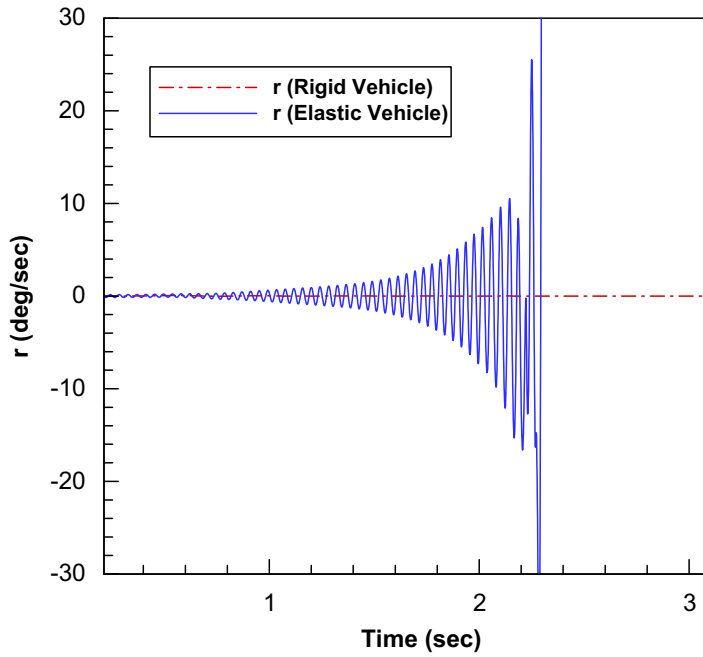


Fig. 14. Yaw angular velocity for rigid and elastic vehicles.

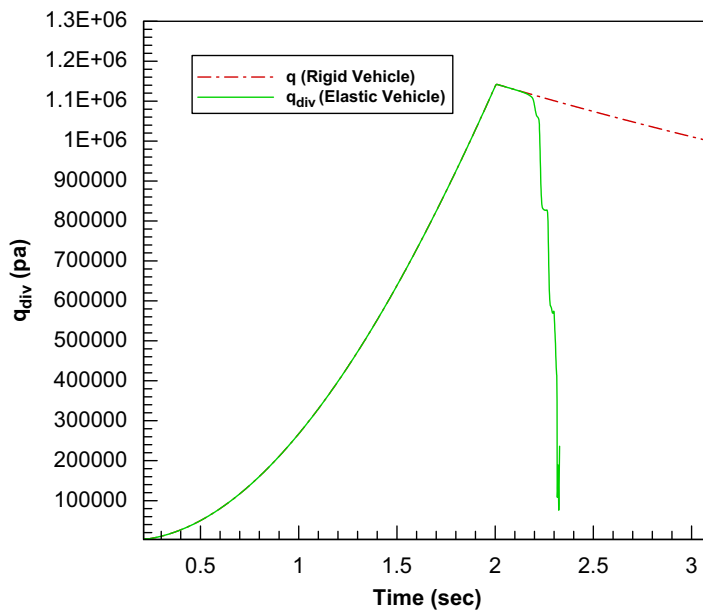


Fig. 15. Dynamic pressure for rigid and elastic vehicles.

Table 9
Comparison table for dynamic pressures equivalent to aeroelastic instabilities.

Vehicle	q_{div} (N/m ²)	Reference
Test Case A	1.149×10^6	Elyada (1989)
Test Case A	1.087×10^6	Haddadpour (2006)
Test Case A	1.013×10^6	Present work

of the vehicle. This behavior of the vehicle is known as an aeroelastic static instability. The same situation for side-slip angle variations versus time can be seen in Fig. 11. In elastic case, the angle of side slip starts fluctuating about rigid stable state and consequently, the vehicle diverges. This phenomenon indicates that the vehicle becomes statically unstable. Pitch angular rates in rigid and elastic cases are shown and compared in Fig. 13. As the figure obviously indicates, the amplitude of oscillations in pitch angular rate increases until the flight vehicle becomes statically unstable and diverges. Obviously, the same behavior can be seen for yaw angular rates of rigid and elastic vehicles in Fig. 14.

The curves of dynamic pressure variations versus time for both cases have been shown in Fig. 15. As can be seen in the figure, either static instability in flight vehicle or increasing drag force, decreases the dynamic pressure of elastic vehicle. In Table 9, the resultant divergence dynamic pressure of the vehicle, investigated in this research, has been compared with the related values from Elyada (1989) and Haddadpour (2006).

5. Conclusions

Equations of elastic motion for a flexible flight vehicle were derived and integrated with the equations of rigid motions. Aerodynamic force and moment coefficients were also determined using the response surface modeling with global nonlinear multivariate orthogonal functions. A database for this work was produced by using a CFD code. The resulting nonlinear analytical formulations for aerodynamic coefficients were used in the equations of motion. In order to develop elastic forces and moments and based on the small elastic deformations, the lift force distribution along the length of the vehicle was considered linear with respect to the single variable α , but nonlinear configurations of all other aerodynamic force and moment coefficients were considered. The n -degree of freedom equations of motion were solved in a prepared flight simulation code by running it for a specific flight vehicle. The results were presented in different tables and graphs. The process of flight simulation is done for unpowered and powered flight conditions for the investigated vehicle in this research. The quantities presented in Elyada (1989) and Haddadpour (2006), such as mass, static margin, dynamic pressure, etc., could be achieved with the model. It was shown that the resultant divergence dynamic pressure coincides with the results of other investigators with a reasonable accuracy. Also from flight simulation results, it is concluded that the elasticity effect causes reduction in static margin and loss of flight static stability.

References

- Attar, P.J., Dowell, E.H., 2005. A reduced order system ID approach to the modeling of nonlinear structural behavior in aeroelasticity. *Journal of Fluids and Structures* 21, 531–542.
- Bisplinghoff, R.L., Ashley, H., 1962. *Principles of Aeroelasticity*. Wiley, New York.
- Chae, S., Hodges, D.H., 2003. Dynamics and aeroelastic analysis of missiles. In: 44th AIAA/ASME/ASCE/AHS Structures, Structural Dynamics, and Materials Conference-10 Norfolk, Virginia.
- Dessi, D., Mastroddi, F., 2008. A nonlinear analysis of stability and gust response of aeroelastic systems. *Journal of Fluids and Structures* 24, 436–445.
- Dinu, A.D., Botez, R.M., Cotoi, I., 2006. Chebyshev polynomials for unsteady aerodynamic calculations in aeroservoelasticity. *Journal of Aircraft* 43, 165–173.
- Elyada, D., 1989. Closed-form approach to rocket vehicles aeroelastic divergence. *Journal of Spacecraft and Rockets* 26, 95–102.
- Gallivan, K.A., 2006. Set 12 Orthogonal Basis Methods. School of Computational Science, Course Note, Florida State University.
- Giraud, L., Langou, J., 2002. Robust selective Gram–Schmidt reorthogonalization. CERFACS Technical Report, TR/PA/02/52.
- Giraud, L., Langou, J., 2005. The loss of orthogonality in the Gram–Schmidt orthogonalization process. *Journal of Computer and Mathematics with Applications* 50, 1069–1075.
- Haddadpour, H., 2006. Aeroservoelastic stability of supersonic slender-body flight vehicles. *Journal of Guidance, Control, and Dynamics* 29, 1423–1429.
- Klien, V., Batterson, J.G., Murphy, P.C., 1981. Determination of airplane model structure from flight data by using modified stepwise regression. NASA TP-1916.
- Meirovitch, L., Nelson, H.D., 1966. On the high-spin motion of a satellite containing elastic parts. *Journal of Spacecraft and Rockets* 3, 1597–1602.
- Meirovitch, L., 1986. *Elements of Vibration Analysis*. McGraw-Hill, New York.
- Meirovitch, L., Tuzcu, I., 2001. Multidisciplinary approach to the modeling of flexible aircraft. In: Proceedings of the CEAS/AIAA/AIAE International Forum on Aeroelasticity and Structural Dynamics, Madrid, Spain, pp. 435–448.
- Meyer, R., 1991. Constructing nonlinear aerodynamic databases. AIAA Paper 91-0552.
- Morelli, A., 1995a. Global Nonlinear Parametric Modeling with Application to F-16. Aerodynamics, Dynamics and Control Branch, NASA Langley Research Center.

- Morelli, A., 1995b. Nonlinear aerodynamic modeling using multivariate orthogonal functions. *Journal of Aircraft* 32, 270–277.
- Morelli, A., DeLoach, R., 2003. Wind tunnel database development using modern experiment design and multivariate orthogonal functions. 41st AIAA Aerospace Sciences Meeting and Exhibit, Reno, NV.
- Nydick, I., Friedmann, P.P., 1998. Aeroelastic analysis of a trimmed generic hypersonic vehicle. AIAA Paper 98-1807.
- Platus, D.H., 1992. Aeroelastic stability of slender, spinning missiles. *Journal of Guidance* 15, 144–151.
- Tang, D., Li, A., Dowell, E.H., 2004. Transient response study on rolling effectiveness of multiple control surfaces. *Journal of Fluids and Structures* 19, 621–634.